Simulations of condensation flows induced by reflection of weak shocks from liquid surfaces

Paolo Barbante and Aldo Frezzotti

Citation: AIP Conference Proceedings **1786**, 110004 (2016); doi: 10.1063/1.4967624

View online: http://dx.doi.org/10.1063/1.4967624

View Table of Contents: http://scitation.aip.org/content/aip/proceeding/aipcp/1786?ver=pdfcov

Published by the AIP Publishing

Simulations of Condensation Flows Induced by Reflection of Weak Shocks from Liquid Surfaces

Paolo Barbante[1] and Aldo Frezzotti[2,a)]

[1]*Dipartimento di Matematica, Politecnico di Milano - Piazza Leonardo da Vinci 32 - 20133 Milano - Italy*
[2]*Dipartimento di Scienze e Tecnologie Aerospaziali, Politecnico di Milano - Via La Masa 34 - 20156 Milano - Italy*

[a)]Corresponding author: aldo.frezzotti@polimi.it

Abstract. The condensation of a vapor onto a planar liquid surface, caused by the reflection of a weak shock wave, is studied by three different simulation method. The first one is based on molecular dynamics (MD) simulations of the Lennard-Jones fluid which are supposed to provide reference solutions. The second method is based on a Diffuse Interface Model (DIM), consistent with the thermodynamic properties of the Lennard-Jones fluid as well as with its transport properties. The third method is based on a hybrid model (HM) in which the liquid is described by a purely hydrodynamic approach, whereas the vapor is described by the Boltzmann equation. The two phases are connected by kinetic boundary conditions. The results show that DIM fails to accurately predict the condensation rate when the vapor is dilute but becomes more accurate when the vapor phase gets denser. HM reproduces MD simulations of nearly ideal vapor condensations with good accuracy, assuming unit condensation coefficient.

INTRODUCTION

At the beginning of the 20*th* century, Korteweg proposed to describe capillary forces by adding to the ordinary expression of the fluid static stress tensor a contribution depending on first and second spatial derivatives of the density field [1]. The resulting equations can accurately describe the liquid-vapor interface in equilibrium conditions. The model can be extended to non-equilibrium flows by adding the Navier-Stokes deviatoric term to the Korteweg static stress tensor [2] and suitable contributions to the classical Fourier law for the heat flux [3], in order to make the model compatible with thermodynamics. The resulting mathematical models for two-phase fluids, named Diffuse Interface Models (DIM), are very attractive. As a matter of fact, a small number of PDEs provide a unified description of the liquid and vapor region, as well as of interfaces, whose formation, merging and destruction are automatically taken into account. Previous studies based on DIM have addressed liquid film instability [4], boiling phenomena [5], bubbles dynamics [6]. A few studies more specifically addressed modeling evaporation and condensation phenomena in simple one-dimensional geometries [7, 8]. In all the studies quoted above, the fluid has been described by Van der Waals equations of state and the reported results, although qualitatively correct, have not been compared to reference experimental or numerical results.

However, it is well known that kinetic layers are present next to liquid-vapor interfaces in non-equilibrium flows [9]. Hence DIM predictions, based on Navier-Stokes-Fourier constitutive laws are not necessarily accurate. A preliminary assessment of DIM predictions in describing the evaporation of a liquid film has been described in Ref. [10], where the predictions of a Diffuse Interface Model consistent with the thermodynamic and transport properties of the Lennard-Jones fluid [11] have been compared to Molecular Dynamics (MD) results. The comparison showed significant deviations of DIM from the reference MD results. Further and more systematic simulations [12] suggest that DIM-MD discrepancies are caused by the poor DIM description of the Knudsen layer and tend to disappear when the vapor phase becomes dense, deviating from the ideal behavior.

The present work aims at completing the assessment by including comparisons about condensation flows. The behavior of DIM is not necessarily the same as in the case of evaporation, since the Knudsen layer has a different structure and the number of free upstream parameters is higher than in the case of evaporation [9, 13]. Accordingly, DIM capabilities are assessed by modeling the quasi-steady condensation which occurs when a shock wave, traveling through the vapor phase, impinges on a liquid surface and is reflected back. Shock reflection from liquid films is a conve-

30th International Symposium on Rarefied Gas Dynamics
AIP Conf. Proc. 1786, 110004-1–110004-8; doi: 10.1063/1.4967624
Published by AIP Publishing. 978-0-7354-1448-8/$30.00

nient way to study condensation processes, not only from the numerical but also from the experimental point of view. The technique has been extensively studied and used to obtain experimental condensation coefficients of various liquids [14, 15]. Here, as in Refs. [10, 12], DIM results are compared with reference MD simulations. For completeness, MD results are also compared with the predictions of a hybrid model (HM) in which the liquid phase is described by continuum equations, whereas the vapor is governed by the Boltzmann equation. The interface is not resolved but the two phases are connected by a quite standard kinetic boundary condition [15, 16].

TEST PROBLEM DESCRIPTION

In the considered test problem, a planar liquid film of thickness Δz_0 initially occupies the region $S_0 = \{(x, y, z) \in R^3 : -\frac{\Delta z_0}{2} \leq z \leq \frac{\Delta z_0}{2}\}$ in the laboratory reference frame. The coordinates x, y span the planes parallel to the vapor-liquid interfaces, whereas the direction along z is perpendicular to them. The liquid slab is initially in equilibrium with its vapor phase at temperature T_l. The vapor phase occupies the region $V_0 = \{(x, y, z) \in R^3 : \frac{\Delta z_0}{2} < |z| < Z_p(0)\}$, union of the two gaps symmetrically located with respect to the origin and delimited by the vapor-liquid interfaces and two infinite, planar and perfectly reflecting pistons, initially located at $\mp Z_p(0)$, respectively. At time $t = 0$ the pistons are impulsively set into motion with constant and subsonic velocities $\pm v_p$ towards the interfaces. As a result of the sudden vapor compression, two shock waves detach from the pistons and start traveling towards the interfaces with constant supersonic speed. The characteristics of the fully developed shocks follow from the Rankine-Hugoniot relationships, being fully determined by v_p. The arrival of the shocks on the liquid surfaces causes the heating of the liquid slab and the reflection of the impinging shocks towards the pistons. In order to control the temperature field in liquid, the center of the liquid slab is kept at constant temperature T_l. After the reflected shock is fully formed, each vapor region can be divided into a thin Knudsen layer, next to the interface, and a uniform equilibrium region of increasing thickness, behind the reflected shock. Here, the temperature T_c and pressure P_c are higher than in the initial equilibrium state, thus causing the vapor to condense onto the liquid surface with subsonic velocity v_c. By a suitable choice of the initial slab thickness and distance of pistons from interfaces, the evolution of the system following shock reflection consists in a fairly uniform increase of the slab thickness, due to quasi-steady condensation. Actually, the temperature profile in the liquid slab, after a short transient phase, takes an almost linear shape determined by T_l, the nearly constant temperature $T_I(t)$ of the interface and the slowly evolving slab thickness $\Delta z(t)$. In this quasi-steady subsonic condensation flow, T_c, P_c and the Mach number $M_c = |v_c|/\sqrt{\gamma R T_c}$ are related by a relationship of the form $\frac{P_c}{P_{sat}(T_I)} = F_{sub}(\frac{T_c}{T_I}, M_c)$ [9]. The form of the function F_{sub}, which determines the condensation rate and the reflected shock properties, crucially depends on the mass, momentum and energy transport through the interfaces [9, 16], hence the problem provides a useful test bench to investigate the capabilities of models to describe such processes.

MOLECULAR DYNAMICS SIMULATIONS OF A LIQUID FILM EVAPORATION

The role of molecular dynamics (MD) [17] simulations is to provide the most fundamental description of the test problem and the reference flowfield properties. It is assumed that the fluid is composed by N_a identical atoms of mass m, interacting pairwise through forces derived from the following Lennard-Jones $6-12$ potential $\phi_{LJ}(r)$ [11]:

$$\phi_{LJ}(r) = 4\epsilon\left[\left(\frac{\sigma}{r}\right)^{12} - \left(\frac{\sigma}{r}\right)^{6}\right] \tag{1}$$

In Eq. (1), r the distance between two interacting atoms, ϵ is the depth of the potential well, whereas the length σ defines the effective range of atomic forces. More precisely, $r_m = 2^{1/6}\sigma$ is the position of the potential minimum. Atomic motions are computed numerically by integrating Newton's equations by the velocity Verlet scheme [17]. The infinite system depicted in Section a) is approximated as the union of periodic replicas of a finite fluid column of fixed side lengths L_x and L_y along the two directions x and y, where periodic boundary conditions [17] are applied, being parallel to the liquid surfaces. Along the direction normal to the liquid surfaces, spanned by the coordinate z, the column height is delimited by the piston positions. Forces have been computed according to the minimum image convention [17], after truncating atomic interactions of pairs whose relative distance r exceeds a specified cut-off radius r_c. A spatial grid, with a cell size of r_c, has been used to index atoms and make the search of nearest neighbors more efficient. Simulations of condensation have been performed by starting each computation from an initial state in which a liquid slab, located in the center of the computational box, is in equilibrium with its vapor at a specified

temperature T_l. A narrow central strip of the liquid slab is thermostatted at temperature T_l by a simple Gaussian thermostat [17]. Local values of the fluid macroscopic quantities have been obtained by sampling microscopic states of atoms belonging to the same spatial cell. The cell system for macroscopic quantities estimation is not the same used for atom indexing, having a resolution of a small fraction of σ. The time evolution of the system macroscopic properties has been obtained by dividing the total simulation duration into a number of time windows and computing time averaged system properties in each window. The amplitude of the time window is small enough to make the interface motion have a negligible effect on sampling spatial profiles. To further increase the number of microscopic samples in the vapor phase, each time snapshot has been obtained by superposing the results of 48 statistically independent parallel simulations of the (macroscopically) same system, each one using from 3×10^4 to 6×10^4 atoms, depending on the simulation conditions. The LJ potential cut-off radius has been set equal to 3.0σ to keep the computational time within reasonable limits. The simulation box lengths L_x and L_y have been set equal to $8r_c$ (or 24σ) for $T_l = 0.72, 0.8$ and reduced to $4r_c$ for $T_l = 1.0$, where the denser vapor phase allows for a smaller simulation box. In the rest of

TABLE 1. Left: Test simulations equilibrium properties values. **Right**: Impinging shock characteristics computed from Rankine-Hugoniot ideal gas relationships. For $T_l = 1.0$, values obtained from MD simulations are enclosed within brackets.

T	ρ_l	ρ_v	l_v	$Z = p/\rho_v T$	T	$\lvert v_p\rvert$	ρ_s/ρ_v	T_s/T_l	M_s	$\lvert v_s\rvert$
0.72	0.803	$5.49e-03$	21.60	0.953	0.72	0.20	1.193	1.126	1.129	1.237
0.80	0.761	$1.226e-02$	11.46	0.914	0.72	0.40	1.402	1.265	1.273	1.394
1.00	0.641	$5.705e-02$	2.473	0.744	0.80	0.20	1.182	1.120	1.122	1.296
					0.80	0.40	1.380	1.2503	1.257	1.452
					1.00	0.20	1.162	1.106	1.109	1.431
							(1.182)	(1.118)	(1.042)	(1.302)

the paper, fluid properties are expressed in Lennard-Jones units, normalizing length, time and mass with respect to σ, $\sqrt{\frac{m\sigma^2}{\epsilon}}$ and m, respectively. Temperature is normalized to $\frac{\epsilon}{k_B}$, being k_B the Boltzmann constant.
MD results reported here have been obtained for $T_l = 0.72, 0.80, 1.0$. Table 1 (left) summarizes the equilibrium properties of the liquid and vapor at the temperatures specified above. The rightmost two columns contain the values of vapor mean free path l_v and compressibility $Z = P_v/(R\rho_v T_l)$, being P_v the vapor pressure, ρ_v the vapor density and $R = k_B/m$ the gas constant. The mean free path has been evaluated from the gas shear viscosity μ, following the dilute gas expression for hard sphere interaction [18]:

$$l_v = \frac{16\mu}{5\sqrt{2\pi R T_l}\rho_v} \tag{2}$$

For the two lower values of T_l the vapor phase is close to ideal behavior, whereas at $T_l = 1.0$ it is not. The right part of Table 1 reports the relevant properties of the shocks generated by the pistons before reflection. The two shocks propagate through the undisturbed vapor with velocities $\pm v_s$, corresponding to a slightly supersonic progation with Mach number M_s. Behind the shock the vapor has the piston speed, density ρ_s and temperature T_s. Shock properties have been computed from Rankine-Hugoniot ideal gas relationships. In the case $T_l = 1.0$ the actual shock properties obtained from MD simulations have been added to ideal ones.

SUMMARY OF DIFFUSE INTERFACE MODEL STRUCTURE AND NUMERICAL TREATMENT

Following Refs. [1, 3, 2], the following set of general conservation laws for mass momentum and energy:

$$\frac{\partial \rho}{\partial t} + \nabla \cdot (\rho \vec{v}) = 0 \tag{3}$$

$$\frac{\partial \rho \vec{v}}{\partial t} + \nabla \cdot (\rho \vec{v} \otimes \vec{v} + \mathbf{P}) = 0 \tag{4}$$

$$\frac{\partial \rho e_T}{\partial t} + \nabla \cdot (\rho e_T \vec{v} + \mathbf{P} \cdot \vec{v} + \vec{q}) = 0 \tag{5}$$

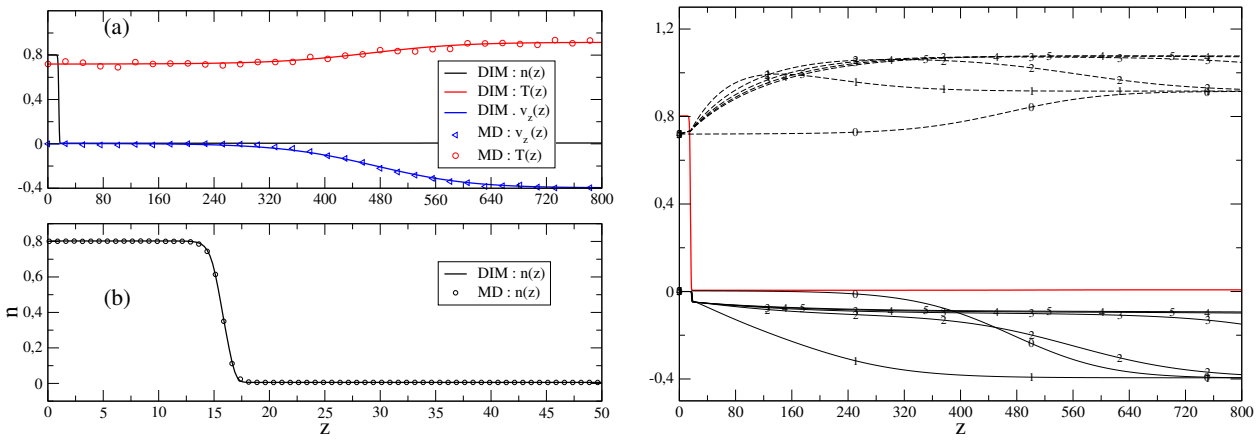

FIGURE 1. Left (a)-Comparison$T_l = 0.72$, $v_p = -0.4$ of MD and DIM density, velocity and temperature profiles before shock-liquid interaction. $T_l = 0.72$, $v_p = -0.4$. **Left** (b) -Comparison of MD and DIM equilibrium density profiles, $T_l = 0.72$. **Right** $T_l = 0.72$, $v_p = -0.4$. Time evolution of DIM computed velocity (solid line) and temperature (dashed lines) profiles. Curves are marked by integer numbers $(0-5)$, following time evolution. The red line represents the initial, undisturbed density profile.

can be given the capability to describe capillary effects through the following closure:

$$\mathbf{P} = \mathbf{P}^{(s)} + \boldsymbol{\tau} \tag{6}$$

$$\boldsymbol{\tau} = -\mu\left(\nabla\vec{v} + \nabla\vec{v}^{T}\right) - \eta\left(\nabla\cdot\vec{v}\right)\mathbf{I} \tag{7}$$

$$\mathbf{P}^{(s)} = \left(p - K\rho\nabla^2\rho - \frac{1}{2}K|\nabla\rho|^2\right)\mathbf{I} + K\nabla\rho\otimes\nabla\rho \tag{8}$$

$$\rho e_T = \rho e + \frac{1}{2}K|\nabla\rho|^2 + \frac{1}{2}\rho v^2 \tag{9}$$

$$\vec{q} = -\lambda\nabla T + K\rho\left(\nabla\cdot\vec{v}\right)\nabla\rho \tag{10}$$

In Equations (6-10), ρ, T, $\vec{v}$, $p(\rho,T)$ and $e(\rho,T)$ are the fluid density, temperature, velocity, hydrostatic pressure and internal energy per unit mass, respectively. The total stress tensor $\mathbf{P}$ is written as the sum of the viscous contribution $\boldsymbol{\tau}$ and the static contribution $\mathbf{P}^{(s)}$. In the expression of the former, $\mu(\rho,T)$ and $\eta(\rho,T)$ are the fluid shear and volume viscosity coefficients, respectively. The expression of $\mathbf{P}^{(s)}$ contains the Korteweg capillary stress correction to the pure hydrostatic pressure, which depends on density spatial derivatives, its intensity being determined by the function $K(\rho,T)$. Consistency with thermodinamics requires that terms associated with density gradients are also added to the total energy density ρe_T definition in Equation (9) and to the classical Fourier contribution $-\lambda\nabla T$ in Equation (10) to obtain the total heat flux $\vec{q}$, being $\lambda(\rho,T)$ the fluid thermal conductivity.
According to the model described above, the equilibrium structure of the planar interface separating two infinite regions, respectively occupied by the liquid and its vapor phase at the common temperature T, is obtained by solving the differential equation

$$P_{zz}^{(s)} = p - K\frac{d^2\rho}{dz^2} + \frac{1}{2}K\left(\frac{d\rho}{dz}\right)^2 = p_\infty \tag{11}$$

$$p_\infty = p(\rho_l,T) = p(\rho_v,T) \tag{12}$$

where the unknown density profile $\rho(z)$ connects the liquid and vapor density values, $\rho_l(T)$ and $\rho_v(T)$, on the vapor-liquid coexistence curve.
In order to build up a Diffuse Interface Model consistent with the properties of the Lennard-Jones (LJ) fluid, the equations of state $p = p(\rho,T)$ and $e = e(\rho,T)$ have been computed from the modified Benedict-Webb-Rubin form, proposed in Ref. [19], which allows an accurate representation of MD data in a wide range of density and temperature. Moreover, simple mean field corrections allow accurately adding the dependence of thermodynamic properties on the LJ potential cutoff distance r_c [19]. Shear viscosity $\mu(\rho,T)$ and thermal conductivity $\lambda(\rho,T)$ have been computed from

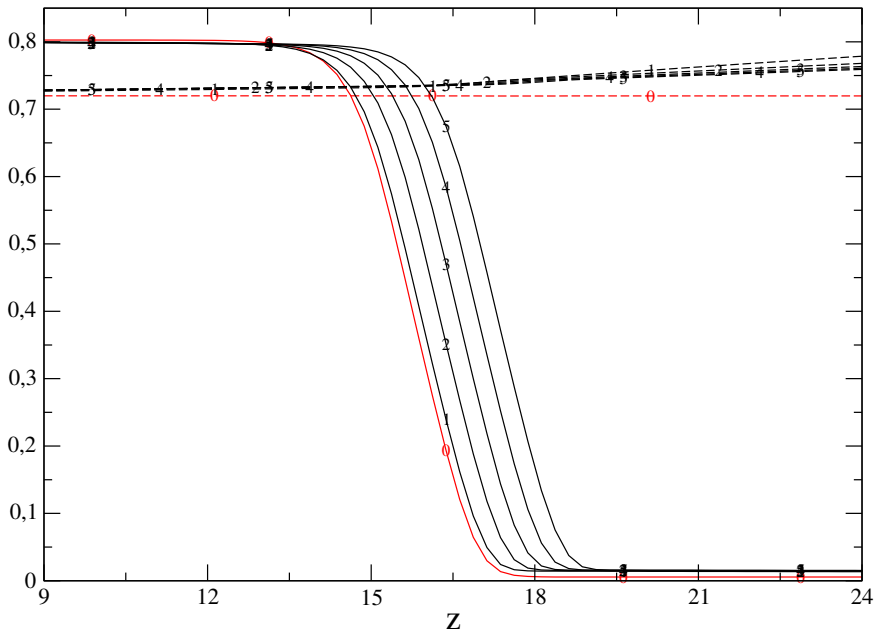

FIGURE 2. $T_l = 0.72$, $v_p = -0.4$. Time evolution of DIM computed density (solid line) and temperature (dashed lines) profiles. Curves are marked by integer numbers $(0-5)$, following time evolution. Red lines represent the initial equilibrium profiles.

the expressions given in Ref. [20] and Ref. [21], respectively. In this study, the contribution of volume viscosity to normal stresses has been neglected because the results suggested that the vapor expansion occurs mainly in the low density flow region where volume viscosity is small. Following the simplification made in most of the studies cited above, the coefficient $K(\rho, T)$ has been assumed not to depend on ρ and T, although its value has been made to depend on T_l. For each computed solution, $K(T_l)$ has been obtained by matching the MD computed equilibrium density profile with the DIM density profile resulting from the integration of Eq. (11). In spite of the simplification, excellent agreement between equilibrium DIM and MD density profiles is obtained by a proper choice of $K(T_l)$ [10, 12].
The governing equations (3), (4) and (5) are discretized in a fixed size domain by a finite volume method based on a staggered one dimensional grid. The mass fluxes that transport momentum and energy are computed from the discretization of continuity equation (3), in such a way momentum and energy, besides mass, are conserved [22]. The transport terms associated with the tensor $\mathbf{P} = \mathbf{P}^{(s)} + \boldsymbol{\tau}$ and the heat flux vector $\vec{q}$ are discretized with a central second order approximation. The convective fluxes are discretized with the second order, non-linear, total variation bounded, upwind OSPRE scheme [23], that ensures a non-oscillatory behavior of the numerical solution. The discretized governing equations are advanced in time with an explicit, second order accurate Runge-Kutta strong stability preserving method [24]. The numerical piston used in MD simulations, is replaced by inflow boundary conditions for density temperature and velocity, whose values are assigned the same values ρ_s, T_s and v_p of the companion MD simulation. The domain extension is wide enough to ensure the onset of a quasi-steady flow behind the reflected shock, before the latter reaches the boundary.

DESCRIPTION AND COMPARISONS OF SIMULATIONS RESULTS

In this section the test problem results, obtained by MD and DIM, are compared. When the initial equilibrium conditions in the vapor are close to ideality ($T_l = 0.72, 0.8$) comparisons are completed with results obtained from a hybrid model (HM) [10, 12] in which the liquid is described by hydrodynamic equations and the vapor phase by the Boltzmann equation, solved by Direct Simulation Monte Carlo (DSMC)[25]. The two phases are separated by a structureless planar interface where standard kinetic boundary conditions are assumed [15, 16], setting evaporation and condensation coefficients equal to one. The model physical properties are consistent with those of the Lennard-Jones fluid adopted for DIM simulations. Figure 1 presents the results obtained by DIM in the case $T_l = 0.72$, $v_p = -0.4$. As shown in the left panels, the free shock profile computed by DIM is in good agreement with the corresponding MD

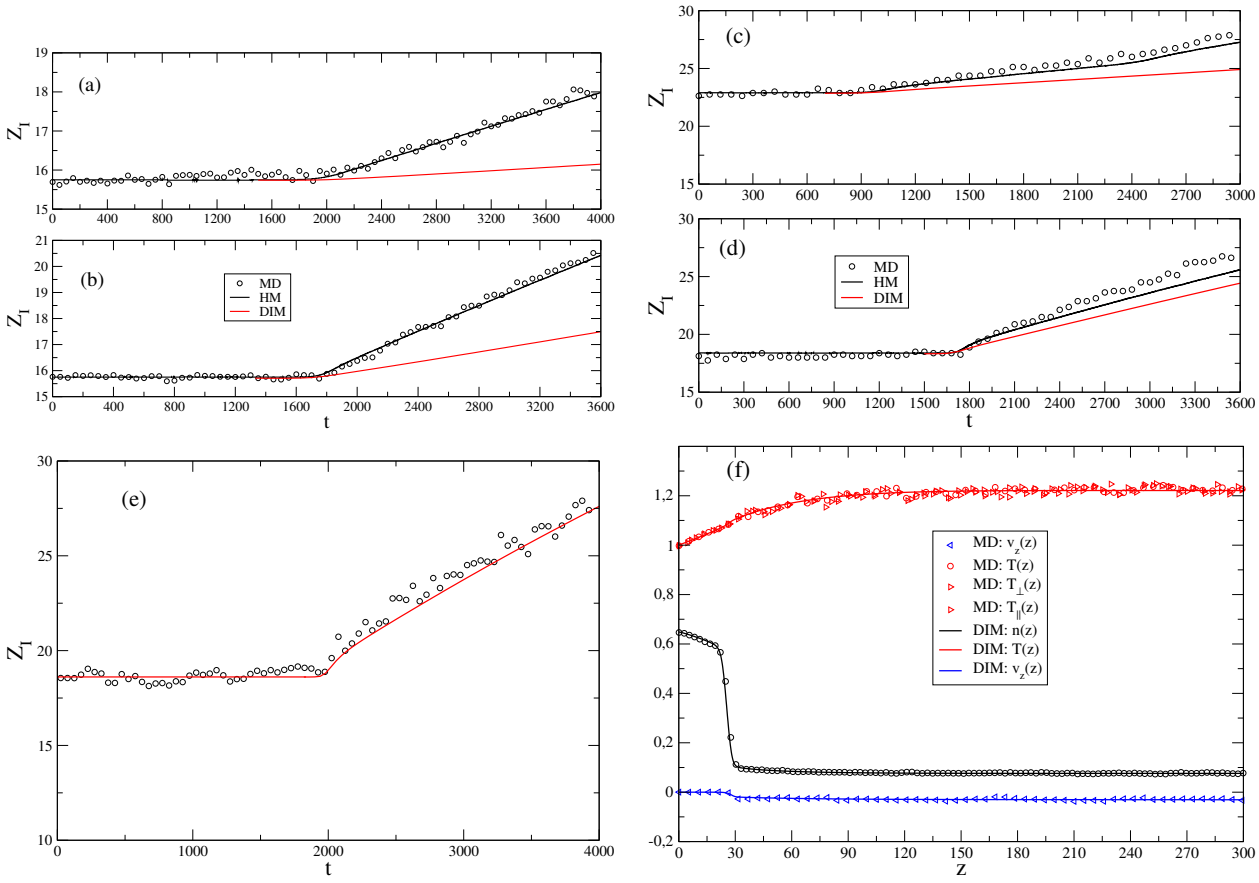

FIGURE 3. Comparisons of MD, DIM and HM time histories of interface position during condensation. ○: MD; Black solid lines: HM; Red solid lines DIM. **(a)** - $T_l = 0.72$, $v_p = 0.2$; **(b)** - $T_l = 0.72$, $v_p = 0.4$; **(c)** - $T_l = 0.8$, $v_p = 0.2$; **(d)** - $T_l = 0.8$, $v_p = 0.4$; **(e)** - $T_l = 1.0$, $v_p = 0.2$; **(f)** Comparison of MD and DIM profiles for $T_l = 1.0$, $v_p = 0.2$

data. The DIM equilibrium density profile is also well fitted to MD profile by choosing the proper value of $K(T_l)$ when solving Equation (11). The time evolution described by DIM is qualitatively correct, as shown in the right panel, where the red line represents the initial, equilibrium density profile. The black solid and dashed lines represent velocity and temperature profiles, respectively. The time evolution shows that, after shock reflection is completed, a quasi-steady flow condition is established in the vapor. If the computational vapor domain is wide enough (a few hundreds mean free paths), the thin Knudsen layer next to the liquid surface is followed by a wide equilibrium region, where gradients are virtually absent and the condensing vapor is characterized by uniform values of density ρ_c, temperature T_c and velocity v_c. As shown in Figure 2, in the liquid velocity is negligible whereas temperature and density profiles evolve quasi-steadily. The former rapidly takes a linear shape which evolves very slowly, following the motion of the interface determined by the liquid density profile which, after an initial transient phase, expands with nearly constant velocity, following the condensation process. Although DIM provides a qualitatively correct picture of the vapor condensation process, the comparison with MD reference data shows discrepancies in the flowfield characteristics after the shock is reflected and quasi-steady conditions set on. Figures 3a-3e compare the MD and DIM time evolutions of interface position $Z_I(t)$ for the conditions listed in Table 1. When the vapor is closer to ideal condition, DIM considerably underestimates the rate of condensation. The DIM computed values of ρ_c, T_c and v_c, reported in Table 2 show that the lower condensation rate is mainly due to signficantly lower velocity v_c. The discrepancies disappear at $T_l = 1.0$ where the high vapor density cancels the temperature jump at the liquid-vapor interface. As shown in Figure 3f, the MD and DIM density, velocity and temperature profiles are in excellent agreement. The time evolution of the interface positions, computed by the two models, are also in very good agreement. The results obtained by the hybrid model, which correctly takes into account the presence of a kinetic layer in the vapor, are in good agreement with the

reference data at $T_l = 0.72$ for both the considered piston speeds. The HM interface evolution is very close to MD results (see Figures 3a,3b). When the liquid temperature and the vapor density increase, deviations of HM data from MD results are observed both in the interface motion (Figures 3c,3d) and in the values of ρ_c, T_c and v_c. However, close to the rarefied regime HM deviates from MD results less than DIM. The behavior of DIM and HM suggests that the deviations of the former from the reference data is related to the presence of the kinetic layer which it cannot describe properly.

TABLE 2. Summary of equilibrium parameters of condensation flow behind the reflected shock as computed by different models

T_l	$\lvert v_p \rvert$	$\rho_c/\rho_v(T_l)$			T_c/T_l			$\lvert v_c \rvert/v_p$		
		MD	DIM	HM	MD	DIM	HM	MD	DIM	HM
0.72	0.2	1.27	1.37	1.27	1.18	1.24	1.18	0.65	0.19	0.63
0.72	0.4	1.62	1.79	1.62	1.39	1.50	1.39	0.59	0.23	0.55
0.80	0.2	1.38	1.34	1.31	1.18	1.22	1.20	0.43	0.25	0.36
0.80	0.4	1.83	1.73	1.69	1.43	1.43	1.43	0.34	0.28	0.32
1.00	0.2	1.34	1.33	-	1.22	1.22	-	0.17	0.18	-

Conclusions

The present study of shock induced condensation flows in the Lennard-Jones fluid follows and completes a previous investigation of the evaporation of a thin planar liquid film [10, 12]. Both studies aim at assessing the accuracy of Diffuse Interface Models in describing evaporation and condensation processes.

As in the case of evaporation, the results obtained so far indicate that significant deviations between MD and DIM flow descriptions are found when the vapor is dilute. The particular DIM implementation adopted in this study is limited by the assumption of constant Korteweg coefficient K. However, previous sensitivity studies in Refs. [10, 12] suggest that the deviations cannot be significantly reduced by varying the constant value or by making it change inside the interface region. The comparison of MD results with those of a hybrid model, which describes the vapor by the Boltzmann equation and the coupling between the liquid and vapor phases by a classical kinetic boundary condition, confirms the good performances of the kinetic approach, already observed in the case of evaporation flows. Furthermore, the comparison suggests that DIM has to be given the capability of describing kinetic layers if good agreement with MD at low vapor densities is desired. One possible direction to be explored is formulating a moment method in the spirit of R13 equations (see Ref. [26] and references therein), in order to improve the description of Knudsen layers. Although more systematic investigations are needed to confirm the obtained results, DIM seems to provide a good description of evaporation/condensation flows when the vapor phase is definitely non-ideal, thus compensating the limitations of the hybrid model.

REFERENCES

[1] D. J. Korteweg, Arch. Néerl. Sci. Exactes Nat. Ser. II **6**, 1–24 (1901).
[2] D. M. Anderson, G. B. McFadden, and A. A. Wheeler, Annu. Rev. Fluid Mech. **30**, 139–165 (1998).
[3] J. Dunn and J. Serrin, Archive for Rational Mechanics and Analysis **88**, 95–133 (1985).
[4] B. Nadiga and S. Zalesky, Eur. J. Mech.,B/Fluids **6**, 885–896 (1996).
[5] A. Onuki, Physical Review E - Statistical, Nonlinear, and Soft Matter Physics **75**, p. 036304 (2007).
[6] F. Magaletti, L. Marino, and C. Casciola, Physical Review Letters **114**, p. 064501 (2015).
[7] D. Bedeaux, E. Johannessen, and A. Røsjorde, Physica A **330**, 329–353 (2003).
[8] V. Babin and R. Hoyst, J. Chem. Phys. **122**, p. 024713 (2005).
[9] Y. Sone, TTSP **29**, 227–260 (2000).
[10] P. Barbante, A. Frezzotti, and L. Gibelli, "A comparison of molecular dynamics and diffuse interface model predictions of lennard-jones fluid evaporation," in *Proceedings of the 29th International Symposium on Rarefied Gas Dynamics*, AIP Conference Proceedings, Vol. 1628, edited by J. Fan (American Institute of Physics, 2014), pp. 893–900.
[11] J.-P. Hansen and I. McDonald, *Theory of Simple Liquids* (Academic Press, London, UK, 2006).
[12] P. Barbante and A. Frezzotti, "A comparison of models for the evaporation of the lennard-jones fluid," (2016), submitted to the European Journal of Mechanics/B Fluids.
[13] Aldo Frezzotti and Tor Ytrehus, Physics of Fluids **18**, p. 027101 (2006).
[14] S. Fujikawa, M. Okuda, T. Akamatsu, and T. Goto, Journal of Fluid Mechanics **183**, 293–324.
[15] S. Fujikawa, T. Yano, and M. Watanabe, *Vapor-Liquid Interfaces, Bubbles and Droplets* (Springer, 2011).
[16] A. Frezzotti, Physics of Fluids **23**, p. 030609 (2011).
[17] M. Allen and D. Tildesley, *Computer Simulation of Liquids* (Clarendon Press, 1989).
[18] S. Chapman and T. G. Cowling, *The Mathematical Theory of Non-Uniform Gases* (Cambridge University Press, Cambridge UK, 1990).
[19] J. K. Johnson, J. A. Zollweg, and K. E. Gubbins, Molecular Physics **78**, 591–618 (1993).
[20] G. Galliero, C. Boned, and A. Baylaucq, Ind. Eng. Chem. Res. **44**, 6963–6972 (2005).
[21] M. Bugel and G. Galliero, Chemical Physics **352**, 249–257 (2008).
[22] J. Ferziger and M. Peric, *Computational Methods for Fluid Dynamics*, 3rd ed. (Springer, 2002).
[23] N. P. Waterson and H. Deconinck, J. of Comput. Phys. **224**, 182–207 (2007).
[24] S. Gottlieb and C. W. Shu, Mathematics of Computation **67**, 73–85 (1998).
[25] G. A. Bird, *Molecular Gas Dynamics and the Direct Simulation of Gas Flows* (Clarendon Press, Oxford, 1994).
[26] A. Rana and H. Struchtrup, Physics of Fluids **28**, p. 027105 (2016).